The Astrophysical Journal, 673:215–225, 2008 January 20

THE STELLAR CONTENT OF GALAXY HALOS: A COMPARISON BETWEEN ΛCDM MODELS AND OBSERVATIONS OF M31

Andreea S. Font,[1,2] Kathryn V. Johnston,[1,3] Annette M. N. Ferguson,[4] James S. Bullock,[5]
Brant E. Robertson,[6,7,8] Jason Tumlinson,[9] and Puragra Guhathakurta[10]
Received 2007 July 4; accepted 2007 October 2

ABSTRACT

Recent observations have revealed that high surface brightness, metal-rich debris is present over large regions of the Andromeda (M31) stellar halo. We use a set of numerical models to determine whether extended metal-rich debris is expected to exist in galaxy halos formed in a hierarchical ΛCDM universe. We identify tidal debris in the simulations according to the current best surface brightness detection limits in M31 and demonstrate that bright features in the outer halo regions usually originate from single satellites, with very little contamination from other sources due to the low probability of tidal streams from two overlapping accretion events. In contrast, high surface brightness features in the inner halo often originate from multiple progenitors. We also compare the age and metallicity distribution of the debris with the well-mixed stellar halos in which they reside. We find that high surface brightness tidal debris is produced almost exclusively by relatively high mass progenitors ($M_* \sim 10^7$–$10^9\ M_\odot$) and thus is expected to be of moderate to high metallicity. Similarly, in our models the smooth inner halo is expected to be metal-rich, as this region has been built up mainly from massive satellites. Our results imply that the stellar populations of substructure observed around external galaxies with current techniques should not resemble old and metal-poor dwarf spheroidal satellites, nor the underlying component of the stellar halo.

Subject headings: cosmology: theory — galaxies: abundances — galaxies: evolution

1. INTRODUCTION

One of the main goals of stellar population studies is to understand the origin of the baryonic components of galaxies. Stellar populations contain a wealth of information—kinematics, age, and chemical abundance—that enables the reconstruction of star formation histories of the past and present-day galaxies. More recently, the growing interest in the topic of "near-field cosmology" (Freeman & Bland-Hawthorn 2002) has raised the question of to what extent stellar populations can be used to constrain cosmological models. In this paper we review recent stellar population data in M31 that appear to challenge hierarchical models of structure formation and compare these data with results of numerical simulations.

Galaxy halos are among the most interesting testing grounds for structure formation theories, as they contain imprints from various star formation episodes, starting with those that took place in the earliest formed structures. Patterns in the stellar populations in different regions of a galaxy halo, or between different halos, or even between halos and their neighboring satellite galaxies, can be analyzed and compared with predictions of cosmological models.

The old and metal-poor halo of our Galaxy has long been the prototype for models of galaxy formation (Searle & Zinn 1978; Laird et al. 1988; Ryan & Norris 1991). Thanks to advances in instrumentational techniques over the last couple of decades it has now become possible to resolve stellar populations in halos of other galaxies within our Local Group: Andromeda (M31)—a galaxy similar in mass and luminosity to our Galaxy (Mould & Kristian 1986; Reitzel et al. 1998; Durrell et al. 2001, 2004; Ferguson et al. 2002, 2005; Brown et al. 2003, 2006a, 2006b, 2007; Ibata et al. 2007)—and various satellite galaxies, such as the Magellanic Clouds, M33, and most of the dwarf spheroidals (Harris & Zaritsky 2001; McConacchie et al. 2006; Mighell & Rich 1996; Hurley-Keller et al. 1998; Gallart et al. 1999; Harbeck et al. 2001; Dolphin 2002; Martin et al. 2006). Whereas the M31 and Milky Way halos exhibit similar stellar compositions (an underlying smooth, metal-poor component and a few metal-rich tidal structures), some local dwarf galaxies are quite different from the large halos. Some of these dwarfs have stellar populations that are on average younger and more metal-rich than the halo of our Galaxy, but overall display a great diversity in their stellar populations (Mateo 1998; Tolstoy et al. 2004; Dolphin et al. 2005).

Recently, it has also become possible to analyze the stellar populations in some of the faintest galactic substructure, namely, in the tidal debris. In contrast with the variety of populations displayed by neighboring dwarf galaxies, the streams discovered so far are striking in their uniformity. Unlike the predominantly old and metal-poor populations of nearby dwarf spheroidal satellite galaxies, the streams discovered so far are predominantly metal-rich with significant intermediate-age components (Ferguson et al. 2005; Brown et al. 2006b). Moreover, the debris has distinct ages and metallicities even in comparison with the surrounding halo in which it resides. In the Milky Way, the Sagittarius stream—the largest substructure discovered in the halo (Ibata et al. 1997; Majewski et al. 1999, 2003)—has significantly younger stars than the stellar halo and an average metallicity that is a few dex higher (Yanny et al. 2000; Ivezić et al. 2000; Martínez-Delgado

[1] Van Vleck Observatory, Wesleyan University, Middletown, CT 06459.
[2] Institute for Computational Cosmology, University of Durham, Science Laboratories, South Road, Durham DH1 3LE, UK.
[3] Department of Astronomy, Columbia University, Pupin Physics Laboratory, 550 West 120th Street, New York, NY 10027.
[4] Institute for Astronomy, University of Edinburgh, Blackford Hill, Edinburgh EH9 3HJ, UK.
[5] Center for Cosmology, Department of Physics and Astronomy, University of California, Irvine, CA 92687.
[6] Kavli Institute for Cosmological Physics, and Department of Astronomy and Astrophysics, University of Chicago, 933 East 56th Street, Chicago, IL 60637.
[7] Enrico Fermi Institute, 5640 South Ellis Avenue, Chicago, IL 60637.
[8] Spitzer Fellow.
[9] Yale Center for Astronomy and Astrophysics, Departments of Physics and Astronomy, Yale University, P.O. Box 208121, New Haven, CT 06520-8121.
[10] UCO/Lick Observatory, Department of Astronomy and Astrophysics, University of California, Santa Cruz, CA 95064.

et al. 2004; Bellazzini et al. 2006; Monaco et al. 2007; Belokurov et al. 2006). An even larger stream dominates the halo of M31 (Ibata et al. 2001). This so-called giant southern stream (GSS) has a mean metallicity of $[\mathrm{Fe/H}] = -0.5$, higher by about 0.2 dex than the inner M31 halo (Ferguson et al. 2002; Guhathakurta et al. 2006), and higher by about 1 dex than the metal-poor M31 halo component (Chapman et al. 2006; Kalirai et al. 2006). The stream also has a larger fraction of intermediate-age stars (Brown et al. 2006a). Other pieces of debris discovered in M31 include the "NGC 205 loop," the "G1 clump," the "North-East shelf," the "Northern spur" (Ferguson et al. 2002, 2005; McConacchie et al. 2004), etc. The latest inventory done by Ibata et al. (2007) in M31 lists about a dozen or so tidal features. Detailed studies of different features in the color-magnitude diagrams in these regions suggest that the metallicities are uniform and high, $[\mathrm{Fe/H}] \sim -0.4$ (Ferguson et al. 2005; Faria et al. 2007).

Are all the data consistent with the hierarchical model for structure formation? At first sight, the diversity of stellar populations in the halos, tidal streams, and surviving satellites is suggestive of a stochastic assembly. However, some of the data have been given another interpretation. For example, it has been argued that the *differences* in chemical abundances between neighboring satellites and the Milky Way halo exclude these satellites from the list of possible halo progenitor types (Venn et al. 2004). At the same time, one can use the *uniformity* of chemical abundances in M31's spheroid as an argument against the hierarchical scenario: if the halo formed from different progenitors, why is the debris so uniform in metallicity (Ferguson et al. 2005)? Other recent observations claiming to challenge the hierarchical scenario use as arguments the apparent lack of very metal-poor stars in some of the surviving dwarf galaxies but not in the stellar halo (Helmi et al. 2006), and the metal-poor component of the M31 extending up to large distances in an apparently homogeneous fashion (Ibata et al. 2007).

From the above arguments, it is clear that better theoretical expectations are needed in terms of the distribution of stellar populations in dwarf galaxies, stellar halos, and the debris. In a recent series of papers we have begun to compare the results of theoretical models with available data, using as a basis a set of simulations of stellar halos formed in a ΛCDM cosmology. We found that the observed differences in $[\alpha/\mathrm{Fe}]$ abundances between the surviving satellites and the halo arise naturally in the ΛCDM framework (Robertson et al. 2005; Font et al. 2006a). We have also shown how the phase-space structure of current debris can be used to recover the merger histories of ΛCDM stellar halos (Font et al. 2006b; K. V. Johnston et al., in preparation) or identify halos whose merger histories are atypical for this cosmology (K. V. Johnston et al., in preparation).

In this paper we make a direct comparison between the stellar populations in our models and those in the halo of M31, down to a level of surface brightness similar to current detection limits. We choose M31 because this galaxy has benefited in recent years from a systematic study of its stellar populations, using either deep *HST* photometry, deep field spectroscopy, or dedicated wide-field surveys (Ferguson et al. 2002, 2005; Brown et al. 2003, 2006a, 2006b, 2007; Guhathakurta et al. 2005, 2006; Irwin et al. 2005; Gilbert et al. 2006, 2007; Kalirai et al. 2006; Ibata et al. 2007; Tanaka et al. 2007). As a result, some aspects of the stellar populations in the M31 halo are known better now than those in the Milky Way, where observations target mainly the solar neighborhood. In addition, M31 exhibits a widespread distribution of metal-rich debris throughout its halo. Our aim is to investigate whether this distribution is consistent with the hierarchical merger model. We use the age-metallicity relation (AMR) as an indicator for the formation of stars in our systems (both in the smooth stellar halo and in the tidal streams). We then compare the AMRs from our simulations with those obtained from the available stellar population data in M31.

We also seek to constrain the origin of the bright, metal-rich debris in stellar halos (and in particular in M31). In observations it is often difficult to disentangle multiple stream components in the debris. In some cases the stars may belong to overlapping orbits of a single satellite (as is now becoming evident in the case of the Sagittarius stream in the Milky Way). In others, the "debris" could be just the perturbed or warped outer disk, as may be the case for some of the recent detections near the edges of M31 and the Milky Way's disks (Momany et al. 2006; Faria et al. 2007). When available, kinematic data can be used to separate the streams in phase space (Helmi & de Zeeuw 2000), and the modeling of orbits can further connect stellar features that are physically separate on the sky. In addition, it is conceivable, although not yet proven, that stellar populations can be used as "tags" for the individual satellites from which they originate. In this paper, we use a statistical sample of bright tidal debris fields to provide a quantitative prediction for their origin. We estimate the average number of satellites per field with significant contributions to the bright debris, both in the inner and outer simulated halos. We also analyze the average metallicity of the bright debris and find that it is in good agreement with the observations in M31.

The paper is structured as follows: In § 2 we summarize the models. In § 3 we present the AMRs of the main galaxy halos (§ 3.1) and of tidal streams (§ 3.2). In § 3.3 we investigate the origin of the highest surface brightness features (§ 3.3.1), and their typical ages and metallicities (§ 3.3.2). In § 4 we make detailed comparisons with available M31 data, for the halo (§ 4.1) and the GSS (§§ 4.2 and 4.2.2). In § 5 we conclude.

2. MODELS

The set of stellar galaxy halos used here has been constructed by Bullock & Johnston (2005) and comprises 11 dark matter halos of mass $M_{\mathrm{vir}} = 1.4 \times 10^{12}\ M_{\odot}$ formed in a ΛCDM universe ($\Omega_m = 0.3,\ \Omega_\Lambda = 0.7,\ h = 0.7$, and $\sigma_8 = 0.9$). For our discussion we also refer to these as L_* galaxy halos.

Full details about the set-up of the simulations can be found in the previous papers (Bullock & Johnston 2005; Robertson et al. 2005; Font et al. 2006a). Here we just briefly summarize the main characteristics of the models. The merger history of the galaxies is based on an extended Press-Schecter formalism (Lacey & Cole 1993), and the evolution of each satellite is followed with a numerical simulation after accretion onto the main halo. The baryonic components are modeled with semianalytical prescriptions. The infall of cold gas into each satellite is followed from the epoch of reionization to the time of its accretion onto the main halo. The gas mass is translated into a stellar mass through a simple star formation prescription, and the stellar profile is assumed to follow a King (1962) model. Star formation ceases soon after accretion onto the main halo, when the gas is assumed to be lost due to ram pressure stripping. The chemical evolution of the accreted substructure is followed with the method of Robertson et al. (2005), which takes into account the enrichment from both Type II and Type Ia supernovae and models feedback as metal-enriched winds from both supernovae and intermediate-mass stars. The models evolve with redshift, but are calibrated only at redshift $z = 0$ to match the stellar mass-metallicity relation, M_*-Z, and the stellar mass−circular velocity relation, M_*-v_{circ}, for Local Group dwarfs.

When evolved to the present day, the models match the main physical properties of the two main galaxies in the Local Group

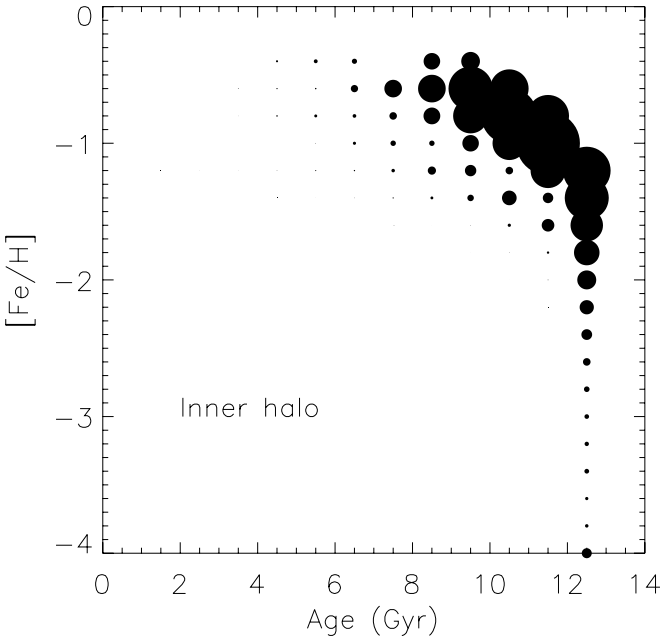

FIG. 1.—AMR for the average of all 11 halos in our sample. Only the inner 50 kpc regions of the halos have been considered here. The area of symbols varies with the mass fraction of stellar populations to the total mass in the field. (No population contributes, by mass, more than 25% to the halo.)

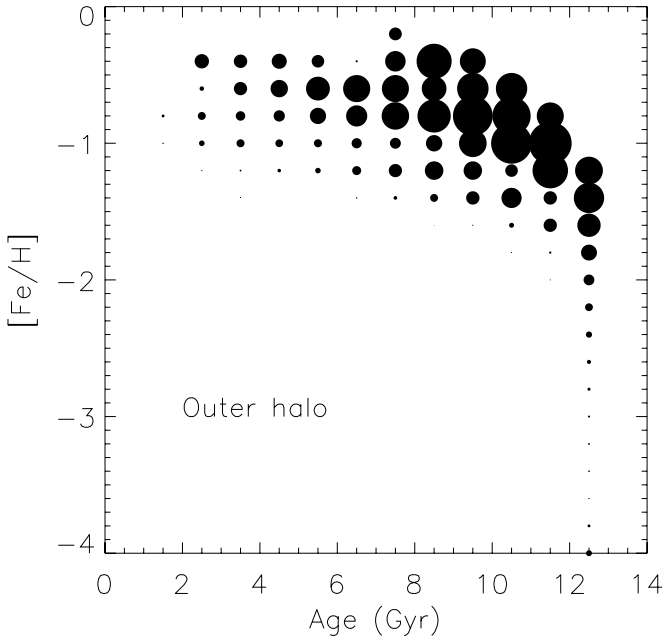

FIG. 2.—AMR for the outer region ($50 < R$ kpc) of the averaged simulated halo. Symbol areas correspond to the stellar mass fraction contributed by the population, as in Fig. 1. The fraction of each population is normalized to the stellar mass of the entire outer halo region.

and of their progenitors: the number of bright ($>10^5\ L_\odot$) surviving satellites per main galaxy, and the masses, density profiles, and total luminosities of the stellar halos are similar to those found in the Milky Way and M31. The average metallicities of our simulated L_*-type galaxy halos range between -1.3 and -0.9. The model also retrieves the differences in the $[\alpha/\mathrm{Fe}]$ abundances between stellar halos and the surviving satellites. More details about the spatial distribution of chemical abundances ([Fe/H] and $[\alpha/\mathrm{Fe}]$) in these stellar halos can be found in Font et al. (2006a, 2006b).

3. RESULTS

3.1. *Predicted Properties of Stellar Halos*

The AMR of a stellar population is a useful tool for gaining insight into the chemical evolution of the system. In a closed box system, it is expected that the oldest populations will be the most metal-poor, whereas the youngest ones the most metal-rich. The slope of the AMR can vary, being generally steeper for the initial stages of the evolution. The AMR will be monotonic only for isolated systems that formed monolithically (Pagel & Patchett 1975; Binney & Merrifield 1998), while systems that formed by accretion of satellites will display a composite functional form, with multiple metallicity components for the same age. In this section we use our models to investigate to what extent the AMR of a stellar halo can be used to place constraints on the galaxy mass assembly history.

Figure 1 shows the AMR of our "typical" stellar halo, constructed by averaging over all 11 halos in our sample. Each symbol represents a cell in the two-dimensional age-[Fe/H] grid in which there are any stars,[11] with the area of the symbol corresponding to the mass fraction contributed by the stellar population to the total stellar mass of the averaged halo. Only the inner 50 kpc of the stellar halos are considered for this plot.

[11] We henceforth consider all stars in a given grid age-[Fe/H] cell to be a distinct stellar population.

The AMR in Figure 1 has a number of distinctive characteristics: (1) the AMR has a single dominant sequence rather than being composed of multiple ones; (2) the sequence is representative of satellites that are massive, i.e., that enrich to $[\mathrm{Fe/H}] > -1$ values in just a few Gyr; and (3) the ages of the stars are typically old, >8 Gyr. These characteristics are a direct consequence of the merger histories of inner halos assumed for our ΛCDM models, and which have been described in more detail in previous papers (Bullock & Johnston 2005; Font et al. 2006a, 2006b). The dominant AMR sequence occurs because the bulk of the inner halo is formed from a few massive satellites (10^7–$10^8\ M_\odot$), even though the main halo accreted satellites with a broader range of stellar masses ($M_* \sim 10^4$–$10^8\ M_\odot$). In addition, massive satellites sink more rapidly into the center due to a more effective drag of dynamical friction. The major contribution to the total stellar mass of massive satellites also explains the clear signature of rapid metal enrichment (more details about the AMRs of individual satellites are given below). Few stars have ages <8 Gyr, and this is because early events dominate the inner halo accretion history.

Spatial variations in the stellar populations' properties across hierarchically formed halo are also of observational interest. Figure 2 shows the AMR of the outer regions of halos ($R > 50$ kpc), using the stellar population data of the same averaged halo as in Figure 1.

The larger spread in ages in the outer halo is a consequence of the late assembly of this region compared with the inner one (Bullock & Johnston 2005; Font et al. 2006a). Given the evolution with time of the typical mass of the accreted systems, the outer halo is formed from satellites with higher masses, $M_* \sim 10^6$–$10^9\ M_\odot$, than the inner halo. Of note is the presence of very massive satellites in the outer halo, $M_* \sim 10^9\ M_\odot$, which extend the outer halo AMR toward $[\mathrm{Fe/H}] \sim 0$ values.

Our results indicate that an averaged sample of the outer halo should display a significantly larger fraction of intermediate-age versus old stars than the inner halo. The metallicity distribution function should also have a broader peak in the outer halo.

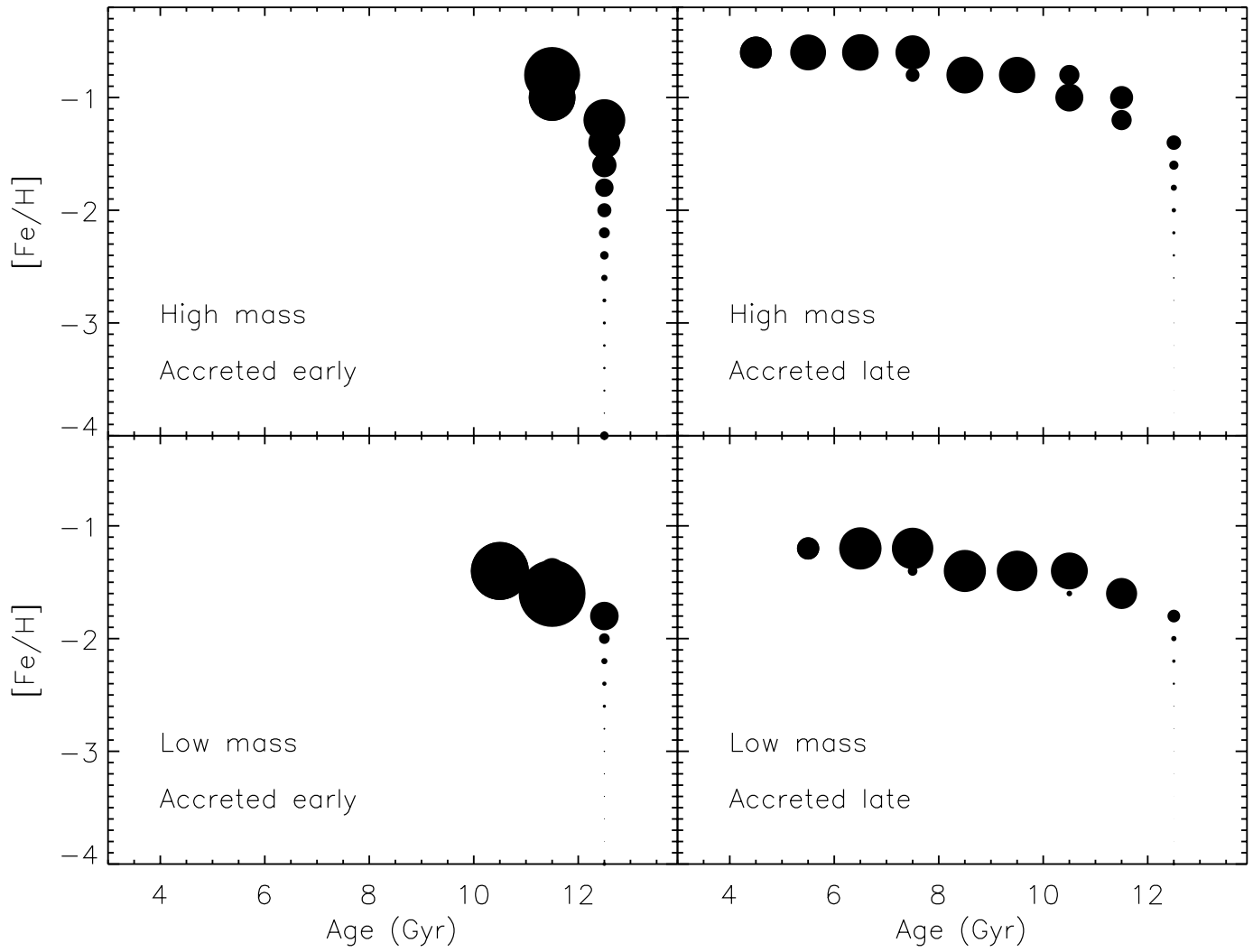

FIG. 3.—AMRs of individual satellites of various masses and accreted at different times. The low-mass satellites chosen here have $M_* \sim 10^6\ M_\odot$, while the high-mass ones have M_* of a few $10^8\ M_\odot$. The accretion times are of 1–2 Gyr for the early events and 6–7 Gyr for the late ones. Symbol areas correspond to the stellar fraction contributed by the population, as in Fig. 1. The stellar mass fractions are normalized to the total stellar mass of each satellite.

3.2. *Predicted Properties of Individual Satellites and Streams*

By construction our simulated satellites have a monotonic chemical enrichment. This limitation results from a number of simplifying assumptions—for example, the merger history of a satellite is approximated with a general formula (Wechsler et al. 2002) and not followed stochastically, and the gas and metals are assumed to be instantaneously mixed after each star formation episode. The predictive power of our models for individual satellites (and streams) is therefore restricted. The individual AMRs will underestimate the scatter in [Fe/H] for stellar populations of the same age. However, our models are fairly reliable in matching the mean metallicity of satellites and the overall AMR sequence.

Figure 3 shows four cases of individual satellites in the range of stellar masses and accretion times that are typically found in our simulations. Despite the limitations in modeling the entire scatter, some trends are obvious. For example, satellites have a smaller [Fe/H] spread at a fixed age than the outer halo, but the spread is comparable to that of the inner halo. Also, the overall shape and maximum [Fe/H] of the inner halo AMR are similar to those of massive satellites ($M_* > 10^8\ M_\odot$).

The AMR of the outer halo contains individual AMR sequences that are more clearly separated (Fig. 2) than those in the inner region of the halo (Fig. 1). As each AMR sequence corresponds to a single satellite or a group of satellites with similar properties, this suggests that using AMRs as a tool to disentangle the accretion histories of stellar halos may be more feasible in the outer rather than the inner regions of the halos.

3.3. *The Extended, High Surface Brightness Debris*

3.3.1. *Origin*

What is the origin of the bright, metal-rich debris extending over large areas in the M31 halo? Was a single satellite responsible for polluting the M31 halo with metal-rich stars or were there several? Here we use our models to constrain the formation history of this debris, assuming that it formed entirely from merging events.

Figure 4 (*top*) shows the surface brightness map of a stellar halo with M31-like properties. The map shows only the surface brightness down to a limit of $\mu_V = 34$ mag arcsec^{-2}, which is roughly the deepest limit achieved currently by wide-field surveys of the M31 (Ferguson et al. 2002; Irwin et al. 2005; Ibata et al. 2007). Figure 4 (*bottom*) shows the surface brightness maps of the main four kinematically cold streams surviving at the present time in the simulated halo.

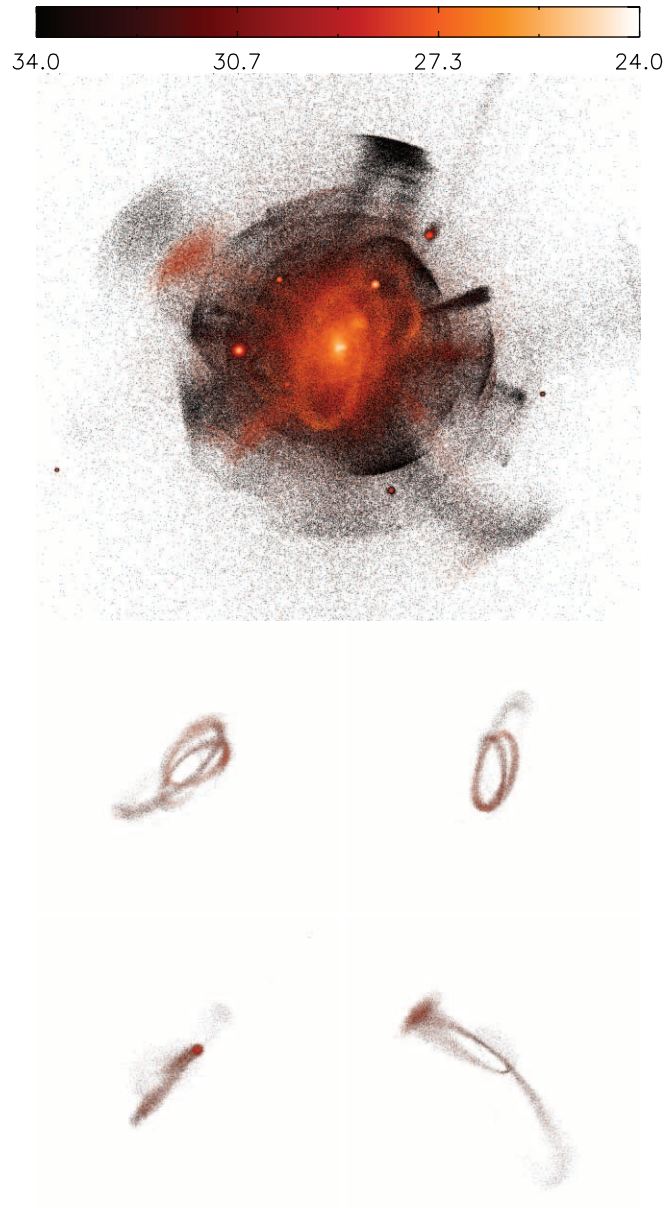

FIG. 4.—*Top*: Stellar halo mapped in surface brightness down to 34 mag arcsec^{-2} (this is halo H2 in Font et al. 2006b). The region shown here extends 150 kpc on the side. *Middle and bottom*: Four examples of kinematically cold streams surviving at present time in the halo above. The streams have been shrunk to a quarter of their size for illustration purposes.

Down to the chosen surface brightness cut, the spatial distribution of the simulated debris is similar to what has been found so far in M31 and the Milky Way: there are a few bright kinematically cold streams (the counterparts of the Sagittarius stream, the GSS, or the NGC 205 loop), the rest of the debris being in the form of much fainter streams or diffuse overdensities.

We define as "high surface brightness" all debris that is as bright as (or brighter than) the current detections of substructure, $\mu_V \sim 30$ mag arcsec^{-2} for the GSS in M31 (Ibata et al. 2001). We therefore select for our analysis all fields which have $\mu_V \leq 30$ mag arcsec^{-2} and that are located on the projected area of a halo along the line of sight. These mock fields have the same area as the pixel size area of the halo map in Figure 4, i.e., 0.4×0.4 kpc. The depth of the field along the line of sight is of the same order as the virial radius of the main galaxy, i.e., $\simeq$300 kpc.

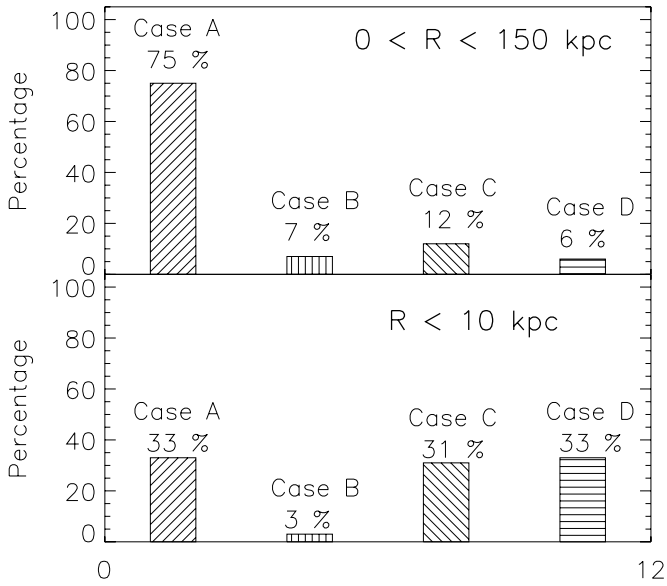

FIG. 5.—Origin of high surface brightness fields ($\mu_V \leq 30$ mag arcsec^{-2}): a single source (case A), two dominant sources (case B), multiple less-dominant sources (case C), and diffuse material originating in many minor sources (case D). *Top*: All bright fields across the halo are selected. *Bottom*: Only the bright fields in the inner $R < 10$ kpc of the halo are selected.

The total surface brightness in each pixel is obtained by integrating over all populations in the field.

We then divide all bright fields into four disjoint cases, based on the formation history of the stellar overdensity in that field:

Case A.—The overdensity originates mainly in a single satellite. The condition we impose is that the satellite contributes a mass fraction $f > 80\%$ of the total stellar mass in the field.

Case B.—The overdensity is formed from contributions of two main satellites. The condition is that these satellites combined contribute more than 80% of the stellar mass in the field.

Case C.—The overdensity is formed from one or more satellites with less significant contribution(s). Specifically, we require that there is at least one satellite contributing $30\% < f < 40\%$, but no satellite contributes more than 40% to the total stellar mass in the field.

Case D.—The overdensity is formed from a multitude of minor satellite contributions. No satellite is contributing more than 30% of the total mass in the field.

Figure 5 (*top*) shows the frequency of each case among the bright fields over the entire area of the stellar halo. Cases in which the overdensity originates in a single satellite (A) occur about 70% of the time, while cases B, C, and D occur less frequently, each about 10% of the time. The actual percentages vary slightly from halo to halo and depend on the imposed surface brightness limit—for example, the frequency of case A increases if we select an even brighter debris. However, case A consistently dominates across the halos. The distribution of these cases begins to reverse in the inner regions of the halos, where phase mixing is more important. Figure 5 (*bottom*) shows the same information as the top panel, but for the inner 10 kpc of the halo. Here, the dominating cases are those in which the debris originates in three or more satellites.

These results have a number of implications for the interpretation of high surface brightness overdensities in galaxies. For example, if the overdensity is relatively distant from the center of the halo, $R > 10$–20 kpc, it is likely to originate in a single satellite, with little contamination from other satellites in the field. This result holds regardless of whether the feature is kinematically

cold or if it is diffused in phase space. For the inner halo, only a third of the bright features are created by a single satellite, the majority of them originating from superposition of streams from three or more satellites (cases C and D).

3.3.2. *Metallicity*

The existence of the metallicity-luminosity relation (Garnett & Shields 1987; Skillman et al. 1989; Brodie & Huchra 1991; Zaritsky et al. 1994) and the corresponding metallicity-mass relation (Lequeux et al. 1979; Tremonti et al. 2004; Erb et al. 2006) for galaxies indicates a connection between the nature of the satellite progenitors and their metallicities. We might expect a corresponding connection to exist between the surface brightness of the current debris and its overall metallicity. Given this expectation, it is useful to examine whether high surface brightness debris in our models (as analog of the M31 observations) indeed originates in satellites of a typical stellar mass, and if so, what is the predicted average metallicity of the debris?

In our models, satellites relatively massive, $M_* \sim 10^7$–$10^8\ M_\odot$, and accreted 10–12 Gyr ago result in sufficiently bright debris to be detected, $\mu_V \sim 30$–32 mag arcsec^{-2} (K. V. Johnston et al., in preparation). As the surface brightness of the debris depends on both the mass of the progenitor, and on the time of accretion, satellites with $M_* \sim 10^7$–$10^8\ M_\odot$ accreted less than 10 Gyr ago are much brighter, $\mu_V \sim 28$–30 mag arcsec^{-2}. Satellites with stellar masses greater than $10^8\ M_\odot$ assemble later and are therefore accreted later (<8 Gyr ago), resulting in debris with the highest surface brightness, $\mu_V \sim 26$–28 mag arcsec^{-2} (K. V. Johnston et al., in preparation). Therefore, the average metallicities of high surface brightness fields originating from a single satellite are expected to range between -1.4 and 0 (which are average values for satellites with stellar masses of 10^7 and $10^9\ M_\odot$, respectively; values are quoted at the time of accretion).

A high surface brightness in a given field can be achieved not only from the contribution of a single relatively massive satellite, but also from the superposition of debris originating in several massive satellites (e.g., if 80% of field stars originating in a 10^7–$10^8\ M_\odot$ satellite reach the detection limit, i.e., a case A, then a combination of two 40% fractions originating in two separate 10^7–$10^8\ M_\odot$ satellites are equally bright, i.e., a case B). In the case of superposition of massive satellites, the average metallicity of the high surface brightness field is similar to the average metallicity of the individual satellites, i.e., the fields are expected to be metal-rich.

As we discuss below, most of the observed debris in M31 *is* metal-rich. The average [Fe/H] in the GSS is approximately -0.5 (Ferguson et al. 2002; Brown et al. 2006b), and other debris throughout the M31 halo have similarly high metallicities, [Fe/H] ~ -0.4 (Ferguson et al. 2005; Faria et al. 2007). In addition, Gilbert et al. (2007) show that the M31 "spheroid" fields and several fields along the minor axis are consistently metal-rich, with and without the cold GSS component. The lesson learnt from our models is that the metal-rich debris currently observed in the inner halo of M31 may not have a single common progenitor, and moreover, each individual inner halo field may contain metal-rich components from multiple sources.

4. APPLICATIONS TO OBSERVATIONS

4.1. *The M31 Halo*

Brown et al. (2006a, 2006b, 2007) have derived the star formation histories at various locations in the outskirts of M31. The resulting ages and metallicities in these fields can be compared directly to our model predictions. A concern is that some of Brown's fields lie along the minor axis of M31, a region that has been shown to contain stars from multiple sources, including the disk and GSS (Ibata et al. 2007). The most recent field analyzed lies at 21 kpc along the minor axis and is expected to have an insignificant contribution from thin disk stars or from the giant extended disk structure detected by Ibata et al. (2005; for evidence against contamination from the latter component, see Gilbert et al. [2007]; also, note that the extended disk component may have an accretion origin as well [Peñarrubia et al. 2006]). On the other hand, the 21 kpc halo field may still be contaminated by stream debris (Gilbert et al. 2007).

We note, however, that from the point of view of hierarchical models one cannot easily differentiate between a "true" or "clean" halo and a halo contaminated by debris. In this context, stellar halos are expected to form through the superposition of tidal debris and show various degrees of phase mixing. Therefore, the only concern in our comparison is not to mistake a field that is dominated by a given stream for one that is representative of the whole halo. The cautionary remark regarding our further comparison with the 21 kpc field of Brown et al. (2007) is that the presence of a cold stream in the inner halo field indeed appears to be atypical in our simulations. Whether this observed field is representative of the whole inner M31 halo, or of a typical Milky Way–type inner halo, remains to be decided by future observations.

Our strategy for further comparisons with the observations is to present averaged results rather than selected, well-matched fields. In this respect, our results do not emphasize the dispersion in stellar population data that can exist among individual halo fields. However, these differences are not expected to be as large in the inner halo as in the less phase-mixed, outer one (Font et al. 2006b).

4.1.1. *The* 21 kpc *Halo Field*

Figure 6 shows a comparison between the 21 kpc halo field of Brown et al. (2007) and our averaged inner halo region (*bottom and top left panels, respectively*). In the right panels we also show the AMR of two individual halos from our sample that have mass accretion histories that bracket the averaged one. (Halo H7 has a protracted mass accretion history, whereas halo H6 has a short one. Halo H7 is also ~0.5 dex more metal-rich than halo H6.)

The dominant presence of old stars in both observations and simulations is not surprising, as inner halos are expected to form within the first few Gyr from the assembly history (Bullock & Johnston 2005). The existence of intermediate-age stars in the inner halos is a new finding that can provide important constraints on the models of halo formation. Brown et al. (2006b) estimate that ~40% of the stars in the field 11 kpc along the minor axis in M31 are less than 10 Gyr old, while the mean age in that field is 9.7 Gyr. Brown et al. (2007) find that the field at 21 kpc along the minor axis has significantly less stars with ages less than 10 Gyr (the fraction is about half of that in the inner field), and virtually no stars with ages less than 8 Gyr. The distribution of populations in the latter field seems to be more in agreement with our models, which predict that about 20% of populations in the inner halo have ages less than 10 Gyr.

The AMRs of the simulated halos show non-negligible populations with intermediate metallicities $-2 <$ [Fe/H] < -1 and ages younger than 10–11 Gyr. Although these populations represent only a minor contribution (<1% by mass) to the entire stellar halo, they can provide important information about the halo formation history. In our models, stars with these ages and metallicities predominantly come from lower mass, metal-poor halo progenitors, and hence are a probe of the accretion of dwarf

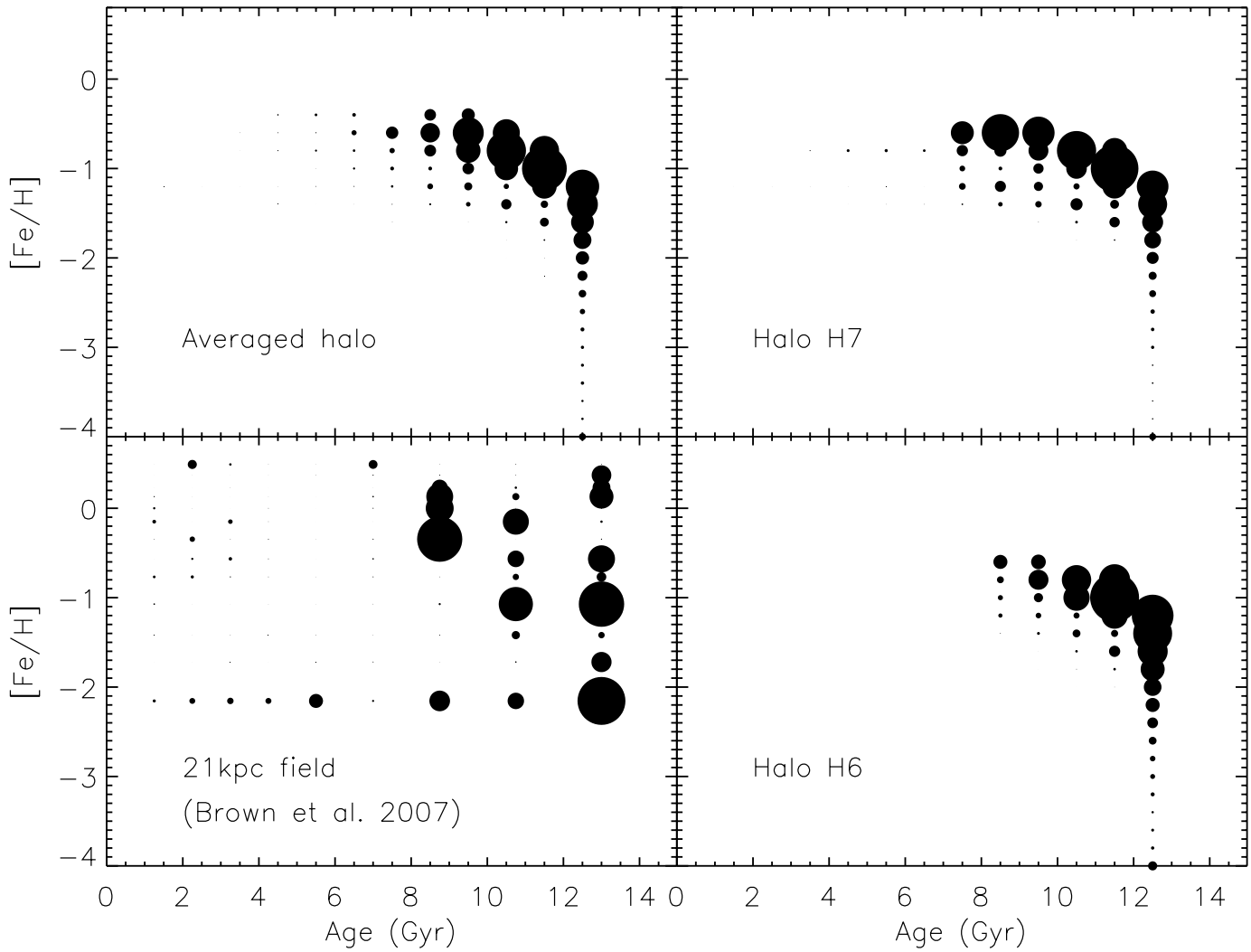

FIG. 6.—Comparison between the halo field of Brown et al. (2007) and simulated inner halo fields. *Top left*: Averaged halo. *Top and bottom right*: Two individual halos with protracted and short mass accretion histories, respectively. *Bottom left*: Observational data (courtesy of T. Brown). The symbol size in the simulated fields is as indicated in Figs. 1 and 2. For the observational data, the area of the circles is proportional to the number of stars in each isochrone group (see Brown et al. 2007).

galaxies at the lower end of the mass function. (Note that the lower metallicity of low-mass halos follows because we imposed that dwarfs accreted today follow the M_*-Z relation; Dekel & Silk 1986; Dekel & Woo 2003.)

The old and metal-poor stars with ages >10 Gyr and $[\mathrm{Fe/H}] < -2$, located in the lower right corners of the AMRs, are good tracers of the early stages of star formation in galaxy halos or in their progenitors. Both our models and the observations show non-negligible fractions of such metal-poor stars (note that the Brown et al. [2007] AMR shows only stars with $[\mathrm{Fe/H}] > -2$, but this may only be an artifact of the limited choice of metallicities in the isochrone data set). At the moment there is a great interest in finding the most metal-poor stars in halos of galaxies and in understanding their origin. Apart from the evidence that the M31 halo has some very metal-poor stars (Brown et al. 2004, 2006b, 2007), the searches also target the Milky Way halo (Beers & Christlieb 2005). In our models most of the stellar populations form in small subhalos at high redshift and enter the main halo in relatively massive satellites. Improved models that track the early episodes of star formation and metal enrichment in more detail will be able to provide better constraints on the origin of this type of populations (see J. Tumlinson et al., in preparation).

Interestingly, the observed AMR of Brown et al. (2007) contains some stars that are more metal-rich than the stars of the same age in our simulated halos (see, in particular, the 8–12 Gyr age interval). This rapid enrichment is indicative of stars originating in a fairly massive satellite, of $\sim 10^9$ or a few 10^8 $M_\odot$ in stellar mass (see, e.g., the AMRs of massive satellites in Fig. 3). The reason that our simulated halos do not show such signatures is that most of the progenitors of these well-mixed regions have stellar masses of 10^7–10^8 $M_\odot$ or less. According to our models, the accretion of a $M_* \sim 10^8$–10^9 $M_\odot$ satellite is a rare event if it were to occur more than 8 Gyr ago. A more recent accretion of such a massive satellite is possible; however, the chances that the satellite is fully disrupted such that it mixes with the rest of the halo are small, unless its orbit is extremely radial. A possible explanation for the origin of these old and metal-rich populations is that they originate in the GSS. (Recall that the 21 kpc field of Brown et al. [2007] *is* contaminated by the GSS, and that the progenitor of the GSS is believed to have been fairly massive and on a radial orbit. See also the discussion of the GSS data in §§ 4.2.1 and 4.2.2.)

There are also a number of discrepancies between our models and the observations of Brown et al. (2007). The stars with ages <5 Gyr and $[Fe/H] > -1$ in the top left corner of the observed AMR cannot be matched by our models. It is, however, unlikely that these extremely young and metal-rich stars belong to the halo. We hypothesize that they are either caused by a very minor contamination by the disk in this field, or belong to a recently accreted stream. The reason that our simulated AMRs do not have this young and metal-rich component is because, *on average*, streams of satellites accreted less than 6 Gyr ago are not found in this inner regions of our simulated halos.

Other more extreme types of populations inferred by Brown et al. (2006b, 2007) in the halo of M31 are also not easily retrieved in our models—for example, the trace populations of young and extremely metal-poor stars (ages <10 Gyr and $[Fe/H] < -2$) in the bottom left corner of the observed AMR or the old and metal-rich stars (ages >10 Gyr and $[Fe/H] > -0.5$) in the top right corner of the same diagram. The reason for this mismatch may be that the modeling of the gas and stellar physics in our models is too simplistic to account for these populations. However, it is difficult to understand what type of satellite systems would have such unusual paths of chemical evolution. In particular, if the young stars with metallicities $[Fe/H] < -2$ do indeed have a merger origin, it implies either that the progenitor satellites formed only recently and in relative pristine environments, or that the mixing of metals inside these satellites was very inefficient. We note, however, that while the presence of these extreme populations was derived from the Brown et al. (2006b) analysis, the authors note themselves that they may not actually be required. Indeed, Brown et al. (2006b) showed that old metal-rich stars could easily be excluded from their model without diminishing the goodness of fit. Furthermore, they point out that what appears as a young metal-poor population in their CMD could at least partially be explained as a population of blue stragglers.

4.1.2. *The Outer Halo*

Figure 2 also shows that the metal-poor populations ($[Fe/H] < -2$) extend out to large distances in the halo, in agreement with recent observations in M31 which detect an underlying metal-poor halo component out to ~150 kpc (Chapman et al. 2006; Gilbert et al. 2006; Kalirai et al. 2006; Ibata et al. 2007).

We find that the ratio of metal-poor stars to metal-rich stars is higher in the outer halo than in the inner one.[12] This result appears to be in agreement with observations that find that the overall metallicity of stars decreases with radius in the M31 spheroid (Bellazzini et al. 2003; Kalirai et al. 2006; Brown et al. 2007). In contrast, the density profiles derived by Irwin et al. (2005) and Ibata et al. (2007) for the metal-poor and metal-rich populations in M31 appear very similar, suggesting that the ratio of these populations is fairly constant from inner to the outer halo.

We also predict that the outer regions of the halos should have, on average, younger ages than the inner ones, as a consequence of the inside-out growth of these halos. The two fields examined by Brown et al. (2007) at 11 and 21 kpc along the minor axis of M31 show an inverse trend. However, it is likely that the excess of younger stars detected in their inner field is the result of contamination by the disk, rather than a genuine trend (however, note that Brown et al. argue against disk contamination in the 11 kpc field). It is certainly desirable to have a detailed analysis of *both* ages and metallicities in more fields across the M31 halo before drawing a definitive conclusion about the age and metallicity gradients in this system.

4.2. *The Giant Southern Stream*

4.2.1. *Stellar Populations*

Figure 7 shows the AMR of the GSS field derived by Brown et al. (2006b) alongside the AMRs of several simulated streams. We have chosen for this comparison only streams that have massive progenitors, $M_* > 10^8\ M_\odot$, as several observational and theoretical studies indicate that this is the case for the GSS progenitor (Ibata et al. 2004; Brown et al. 2006a; Font et al. 2006c). For example, we find that only progenitors with total stellar masses greater than $\sim 5 \times 10^8\ M_\odot$ are able to match the most metal-rich portion of the observed AMR. Among these massive satellites, we find that those accreted ~6–7 Gyr ago provide a better fit to the observed AMR (e.g., Fig. 7, *bottom left*) and also result in tidal debris of comparable surface brightness as the GSS, $\mu_V \sim 30$ mag arcsec^{-2} (Ibata et al. 2001). (A more detailed discussion about constraining the time of accretion is given in § 4.2.2.)

The AMRs of satellites accreted 6–7 Gyr ago also have about 70% of their stars younger than 10 Gyr, in agreement with what has been found in the GSS (Brown et al. 2006b).

Not all stellar population data can be matched by our models. The metal-poor populations ($[Fe/H] < -2$) are not as significant in the simulated AMR as in the stream field of Brown et al. (2006b). Also, as in the case of main halos, the most extreme populations detected in the GSS field, such as the top right, top left, and bottom left corners of the age-[Fe/H] grid of Brown et al. (2006b) are inconsistent with our chemical evolution models.

As discussed before, the mismatch between the observations and the models can be attributed, in part, to the limitations of our current modeling of individual streams. In addition, the observational data in the GSS field may contain stars from other components, such as the disk, other tidal debris, or the background halo. For instance, Brown et al. (2006b) estimate that about 25% of the stars in the stream field could belong to the underlying halo. In addition, as previously discussed in § 4.1.1, some of these extreme populations, such as the old and metal-rich ones, are not necessarily required for a good fit to the observations (although the young and metal-poor ones seem to be required).

4.2.2. *Constraining the Time of Accretion*

Although the constraints on the mass of the GSS progenitor are fairly good, the time of accretion is largely uncertain.[13] Here we discuss the possibility of putting some constraints on the latter by using our star formation history models.

Even though stellar population data contain direct information only about the star formation history of the progenitor galaxy, indirectly they can also provide some constraints on the external mechanisms that can shut off star formation. The accretion of the satellite onto the main halo is such a mechanism that may affect the star formation process within the satellite, slowing it down or stopping it completely. Brown et al. (2006b) suggested that the cessation of star formation in the GSS ~6–7 Gyr ago might have coincided with the accretion of the progenitor satellite onto the M31. For example, if the satellite were accreted earlier than 7 Gyr ago, ram pressure stripping along this highly eccentric orbit could have removed the gas reservoir and therefore stopped the star formation earlier than it is observed. Similarly, if the satellite were

[12] This result does not imply that the *absolute* number of metal-poor stars in outer halo should be higher than in the inner halo. The density of metal-poor stars is expected to decrease with distance from the center of the galaxy (see Font et al. 2006b).

[13] The time of accretion is defined here as the time when the satellite enters the virial radius of the host galaxy.

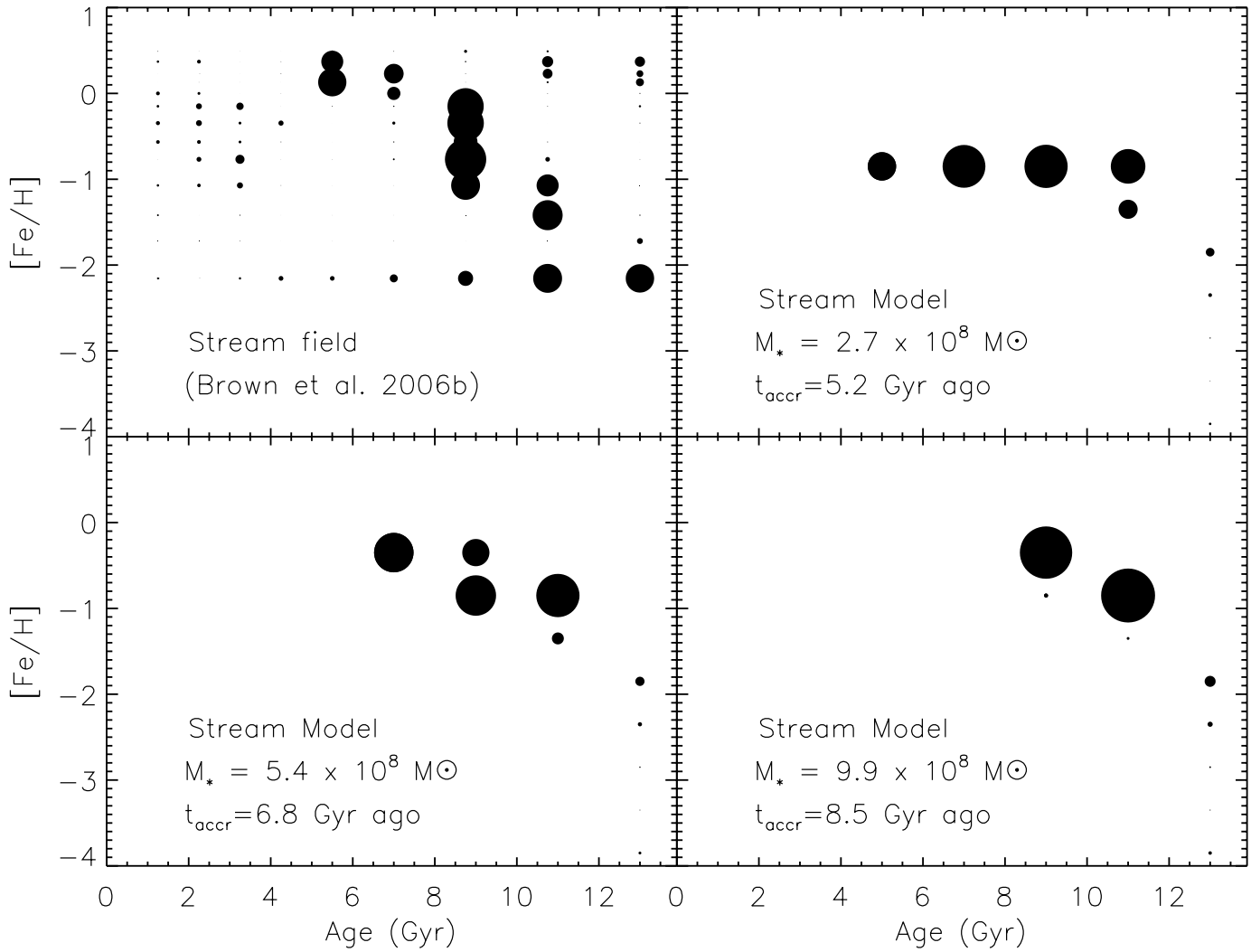

FIG. 7.—Comparison between the GSS field of Brown et al. (2006b) and several simulated streams (observational data are courtesy of T. Brown). The symbol size in the simulated streams is as indicated in Fig. 3. For the observational data, the area of the circles is proportional to the number of stars in each isochrone group (see Brown et al. 2006b).

accreted more recently, star formation would have continued several Gyr after what is observed, unless some intrinsic mechanism would have stopped it before the accretion.

However, a time of accretion of 6–7 Gyr ago is at odds with current numerical modeling of the satellite orbit that fits the kinematic data. The simulations find that the progenitor satellite has spent less than 1 Gyr orbiting from the farthest location along the stream until the current pericenter (Ibata et al. 2004; Fardal et al. 2006, 2007; Font et al. 2006c; Geehan et al. 2006), and assuming that farthest edge of the stream is the point where the satellite was accreted, it implies that the satellite must have been accreted within the last ~1 Gyr.

Although the stellar population data cannot provide stringent constraints on the dynamical evolution of the satellite, the arguments above point toward a possible conflict with the numerical estimates. We examine below two possibilities: first, that the progenitor was accreted recently (<1–2 Gyr ago) but the star formation stopped several Gyr prior to that; and second, that the satellite was accreted 6–7 Gyr ago.

In the first case, the question is how likely is it that star formation stops several Gyr prior to the accretion, particularly in a fairly massive satellite, as is inferred to be the case for the progenitor of the GSS. In Figure 8 we investigate this scenario quantitatively, by selecting all satellites accreted less than 7 Gyr ago and plotting the fraction of stars formed in the 4 Gyr time interval before accretion. The satellites are divided into three categories depending on their time of accretion: satellites accreted about 5–7 Gyr ago, satellites accreted recently (<2.5 Gyr), and satellites accreted at intermediate times. The fraction of stars is expressed as a function of the total stellar mass of the satellite at the time of accretion. For more massive satellites, $M_* > 10^7\ M_\odot$—as is assumed for the progenitor of the GSS—at least 40% of all their stars are formed within the 4 Gyr before accretion. The implication is that, if the progenitor were indeed accreted within the last 1–2 Gyr, the observations should detect a ~40% fraction of young stars (ages <6 Gyr). Current observations, however, do not detect such a high fraction of young stars (Brown et al. 2006b).

Therefore, the results based on our models seem to concur that, for a massive satellite, a time of accretion of 1–2 Gyr ago is difficult to reconcile with a cessation of star formation 4 Gyr prior to that. The caveat, of course, is that the star formation prescription in our models may be too simplistic. The alternative is that the progenitor of the GSS was indeed accreted 6–7 Gyr ago. In this case, it is likely that the satellite orbited more than once in the M31 halo, as the time taken to complete an orbit with the current kinematic properties is much less than 6–7 Gyr (see the numerical

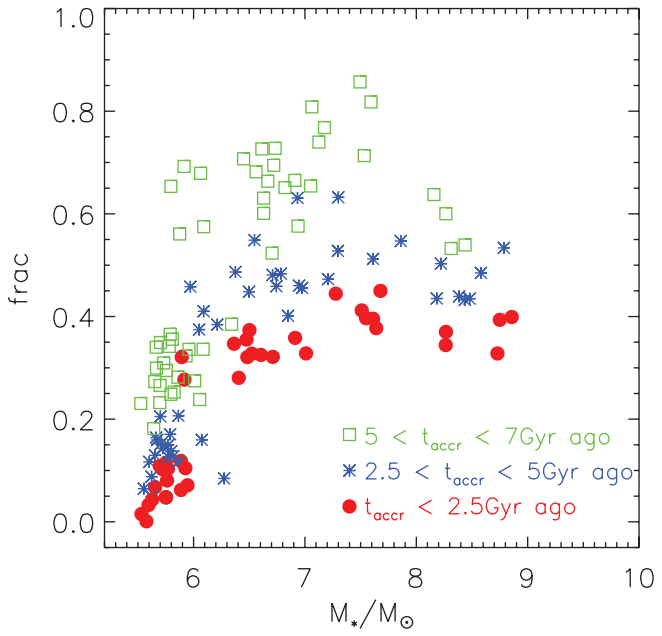

FIG. 8.—Fraction of stars formed in the 4 Gyr before the time of accretion in simulated satellites as a function of the total stellar mass of the satellite. Different symbols represent different accretion times: less than 2.5 Gyr ago (*red circles*), between 2.5 and 5 Gyr (*blue stars*), and between 5 and 7 Gyr ago (*green squares*).

simulations of Ibata et al. 2004; Fardal et al. 2006, 2007; Font et al. 2006c; Geehan et al. 2006). Also, it is unlikely that a tidal stream that detached 7 Gyr ago would still survive today as a coherent feature. Therefore, if the satellite was accreted 6–7 Gyr ago, the stars in the current stream must have been tidally stripped from the parent halo relatively recently. It is possible that a resolution between the results of numerical modeling and stellar population data can be achieved if the starting point of simulations is moved beyond the edge of the currently detected stream. Extrapolating the numerical parameter space in regions which are not constrained by the data would be difficult, but certainly worth doing. The task of constraining the orbital parameters could be greatly eased if future observations find a continuation of the stream beyond the current edge, either along this orbit or on a previous one.

Our current simulations can provide some predictions on how faint the streams of satellites that undergo multiple orbits should be. The small panels at the bottom of the Figure 4 illustrate the surface brightness of a few streams formed when the parent satellite is at its first and then second passage inside the main halo. The streams are brightest when they just form, then become faint with time. Therefore, the streams that formed in a recent passage of a satellite inside the main halo are expected to be brighter than the streams that survive from previous a orbit of that satellite (however, the effect is attenuated by the fact that more stellar material is stripped at earlier passages of the satellite, therefore the *initial* surface brightness of the streams is higher for the streams formed earlier). We find that while the brighter (i.e., more recently detached) streams have an average surface brightness of $\sim$25–26 mag arcsec^{-2}, the fainter counterparts have, on average, $\mu_V \sim 26$–27 mag arcsec^{-2}. These surface brightness levels should be achievable with current detection limits.

5. CONCLUSIONS

In this paper we used a set of simulations of stellar halos of L_* galaxies to study the composition of their stellar populations and provide comparisons with the observations. The test case for our comparisons was M31, given the wealth of data that exists for this galaxy. However, we emphasize that the theoretical results derived here are applicable to any large $\sim L_*$ galaxy and therefore provide a framework for interpreting the substructure of such galaxies that will be uncovered in upcoming surveys.

The main conclusions of our study are as follows:

1. The global stellar populations of halos assembled hierarchically will vary according to their different accretion histories. For example, the presence of metal-rich debris in a galaxy like M31 suggests a history that included the accretion of at least one massive satellite. Conversely, the more metal-poor halo of the Milky Way is evidence that its progenitor satellites were less massive than those of M31.
2. The homogeneous high metallicity in the inner M31 halo found by Brown et al. (2007) can be naturally explained in the context of hierarchical merging. According to our models the homogeneity of stellar populations occurs because the inner halo is dominated by a few massive satellites, $M_* \simeq 10^7$–$10^8\ M_\odot$, which had very similar star formation and chemical evolution histories. The predicted imprint of these satellites in the inner stellar halo is the presence of old stars with $[\mathrm{Fe/H}] > -1$.
3. The outer halos in our models tend to have a larger spread in the ages and metallicities of stellar populations than the inner parts. This diversity may not be apparent in current observations because the spread is contributed in part by a multitude of low surface brightness features. Ongoing deep observations in M31 should be able to test this prediction.
4. We have investigated the origin of high surface debris in different regions of the halo. The debris in the outer $R > 10$ kpc halo typically originates in single massive satellites. This result holds regardless of whether the debris is kinematically cold or it is diffuse in phase space. The outer regions give the best opportunity of reconstructing the formation history of stellar halos, as their stellar populations retain information about the nature of the mergers in a nondegenerate form.
5. The origin of bright debris in the inner 10 kpc halo is more varied. Here tidal debris from a single massive progenitor or a superposition of debris from several large or small satellites can result in similar surface brightness levels. Disentangling the complex formation histories of these fields is possible, provided that the interpretation of observational data takes into account the predictions of hierarchical models.
6. The brightest tidal debris (i.e., that can be observed with current surface brightness limits) still orbiting around M31 or Milky Way–type galaxies should be metal-rich. Therefore, it should not be expected to resemble the characteristically old and metal-poor stellar populations of dwarf spheroidal satellites, nor those of the smooth underlying halo.
7. We illustrated the case of GSS in M31, whose progenitor was a massive dwarf galaxy accreted more recently than the main progenitors of the halo. The presence of intermediate-age stars and the absence of young stars suggest that the satellite could have been accreted as long ago as 6–7 Gyr. If the satellite was accreted more than 1–2 Gyr ago, a continuation of the stream should exist in the halo of M31, about 1–2 mag arcsec^{-2} fainter than the currently observed one.

We thank the referee for a thorough reading of the manuscript and for useful suggestions that improved the presentation of our paper. We wish to thank Tom Brown for providing us with

observational data for the halo and stream fields in M31. We also thank Tom Brown, Henry Ferguson, and Karrie Gilbert for helpful conversations and the Aspen Center for Physics for hospitality during the writing of this paper. Support for programs GO-9458 and GO-10128 was provided by NASA through a grant from the Space Telescope Science Institute, which is operated by the Association of Universities for Research in Astronomy, Inc., under NASA contract NAS5-26555. A. S. F. and K. V. J.'s contributions were supported through the NSF CAREER award AST 01-33617. A. S. F. is supported by a PPARC Fellowship at the Institute for Computational Cosmology in Durham. A. M. N. F. is supported by a Marie Curie Excellence Grant from the European Commission under contract MCEXT-CT-2005-025869. B. E. R. gratefully acknowledges the support of a *Spitzer* Fellowship through a NASA grant administered by the *Spitzer* Science Center. J. T. gratefully acknowledges the generous support of Gilbert and Jaylee Mead for their namesake fellowship in the Yale Center for Astronomy and Astrophysics. P. G. acknowledges support from NSF grants AST 03-07966 and AST 05-07483 and NASA/STScI grants GO-10265.02 and GO-10134.02.

REFERENCES

Beers, T. C., & Christlieb, N. 2005, ARA&A, 43, 531
Bellazzini, M., Cacciari, C., Federici, L., Fusi Pecci, F., & Rich, M. 2003, A&A, 405, 867
Bellazzini, M., Newberg, H. J., Correnti, M., Ferraro, F. R., & Monaco, L. 2006, A&A, 457, L21
Belokurov, V., et al. 2006, ApJ, 642, L137
Binney, J., & Merrifield, M. 1998, Galactic Astronomy (Princeton: Princeton Univ. Press)
Brodie, J. P., & Huchra, J. P. 1991, ApJ, 379, 157
Brown, T. M., et al. 2003, ApJ, 592, L17
———. 2004, AJ, 127, 2738
———. 2006a, ApJ, 636, L89
———. 2006b, ApJ, 652, 323
———. 2007, ApJ, 658, L95
Bullock, J. S., & Johnston, K. V. 2005, ApJ, 635, 931
Chapman, S., et al. 2006, ApJ, 653, 255
Dekel, A., & Silk, J. 1986, ApJ, 303, 39
Dekel, A., & Woo, J. 2003, MNRAS, 344, 1131
Dolphin, A. E. 2002, MNRAS, 332, 91
Dolphin, A. E., Weisz, D. R., Skillman, E. D., & Holtzman, J. A. 2005, in ASP Conf. Ser., Resolved Stellar Populations, ed. D. Valls-Gabaud & M. Chavez (San Francisco: ASP), in press
Durrell, P. R., Harris, W. E., & Pritchet, C. J. 2001, AJ, 121, 2557
———. 2004, AJ, 128, 260
Erb, D. K., et al. 2006, ApJ, 644, 813
Fardal, M. A., Babul, A., Geehan, J. J., & Guhathakurta, P. 2006, MNRAS, 366, 1012
Fardal, M. A., Guhathakurta, P., Babul, A., & McConnachie, A. W. 2007, MNRAS, 380, 15
Faria, D., et al. 2007, AJ, 133, 1275
Ferguson, A. M. N., Irwin, M. J., Ibata, R. A., Lewis, G. F., & Tanvir, N. R. 2002, AJ, 124, 1452
Ferguson, A. M. N., et al. 2005, ApJ, 622, L109
Font, A. S., Johnston, K. V., Bullock, J. S., & Robertson, B. E. 2006a, ApJ, 638, 585
———. 2006b, ApJ, 646, 886
Font, A. S., Johnston, K. V., Guhathakurta, P., Majewski, S. R., & Rich, R. M. 2006c, AJ, 131, 1436
Freeman, K., & Bland-Hawthorn, J. 2002, ARA&A, 40, 487
Gallart, C., Freedman, W. L., Aparicio, A., Bertelli, G., & Chiosi, C. 1999, AJ, 118, 2245
Garnett, D. R., & Shields, G. A. 1987, ApJ, 317, 82
Geehan, J. J., Fardal, M. A., Babul, A., & Guhathakurta, P. 2006, MNRAS, 366, 996
Gilbert, K. M., et al. 2006, ApJ, 652, 1188
———. 2007, ApJ, 668, 245
Guhathakurta, P., et al. 2005, preprint (astro-ph/0502366)
———. 2006, AJ, 131, 2497
Harbeck, D., et al. 2001, AJ, 122, 3092
Harris, J., & Zaritsky, D. 2001, ApJS, 136, 25
Helmi, A., & de Zeeuw, P. T. 2000, MNRAS, 319, 657
Helmi, A., et al. 2006, ApJ, 651, L121
Hurley-Keller, D., Mateo, M., & Nemec, J. 1998, AJ, 115, 1840
King, I. 1962, AJ, 67, 471
Ibata, R. A., Chapman, S., Ferguson, A. M. N., Irwin, M., Lewis, G. F., & McConnachie, A.. 2004, MNRAS, 351, 117
Ibata, R. A., Chapman, S., Ferguson, A. M. N., Lewis, G. F., Irwin, M., & Tanvir, N.. 2005, ApJ, 634, 287
Ibata, R. A., Irwin, M., Lewis, G., Ferguson, A. M. N., & Tanvir, N. 2001, Nature, 412, 49
Ibata, R. A., Wyse, R. F. G., Gilmore, G., Irwin, M. J., & Suntzeff, N. B. 1997, AJ, 113, 634
Ibata, R. A., et al. 2007, ApJ, submitted (arXiv: 0704.1318v1)
Irwin, M., Ferguson, A. M. N., Ibata, R., Lewis, G. F., & Tanvir, N. R. 2005, ApJ, 628, L105
Ivezić, Ž., et al. 2000, AJ, 120, 963
Kalirai, J. S., et al. 2006, ApJ, 648, 389
Lacey, C., & Cole, S. 1993, MNRAS, 262, 627
Laird, J. B., Carney, B. W., Rupen, M. P., & Latham, D. W. 1988, AJ, 96, 1908
Lequeux, J., Rayo, J. F., Serrano, A., Peimbert, M., & Torres-Peimbert, S. 1979, A&A, 80, 155
Majewski, S. R., Siegel, M. H., Kunkel, W. E., Reid, I. N., Johnston, K. V., Thompson, I. B., Landolt, A. U., & Palma, C. 1999, AJ, 118, 1709
Majewski, S. R., Skrutskie, M. F., Weinberg, M. D., & Ostheimer, J. C. 2003, ApJ, 599, 1082
Martin, N. F., et al. 2006, MNRAS, 371, 1983
Martínez-Delgado, D., Gómez-Flechoso, M. A., Aparicio, A., & Carrera, R. 2004, ApJ, 601, 242
Mateo, M. 1998, ARA&A, 36, 435
McConacchie, A. W., et al. 2004, MNRAS, 351, L94
———. 2006, ApJ, 647, L25
Mighell, K. J., & Rich, M. 1996, AJ, 111, 777
Momany, Y., et al, 2006, A&A, 451, 515
Monaco, L., et al. 2007, A&A, 464, 201
Mould, J., & Kristian, J. 1986, ApJ, 305, 591
Pagel, B. E. J., & Patchett, B. E. 1975, MNRAS, 172, 13
Peñarrubia, J., McConnachie, A. W., & Babul, A. 2006, ApJ, 650, L33
Reitzel, D. B., Guhathakurta, P., & Gould, A. 1998, AJ, 116, 707
Robertson, B., Bullock, J. S., Font, A. S., Johnston, K. V., & Hernquist, L. 2005, ApJ, 632, 872
Ryan, S. G., & Norris, J. E. 1991, AJ, 101, 1865
Searle, L., & Zinn, R. 1978, ApJ, 225, 357
Skillman, E. D., Kennicutt, R. C., & Hodge, P. W. 1989, ApJ, 347, 875
Tanaka, M., Chiba, M., Komiyama, Y., Iye, M., & Guhathakurta, P. 2007, ApJ, submitted (arXiv: 0704.3328)
Tolstoy, E., et al. 2004, ApJ, 617, L119
Tremonti, C. A., et al. 2004, ApJ, 613, 898
Venn, K. A., Irwin, M., Shetrone, M. D., Tout, C. A., Hill, V., & Tolstoy, E. 2004, AJ, 128, 1177
Wechsler, R. H., Bullock, J. S., Primack, J. R., Kravtsov, A. V., & Dekel, A. 2002, ApJ, 568, 52
Yanny, B., et al. 2000, ApJ, 540, 825
Zaritsky, D., Kennicutt, R. C., & Huchra, J. P. 1994, ApJ, 420, 87